ELSEVIER

Chemistry and Physics of Lipids
89 (1997) 31–44

CPL
CHEMISTRY AND PHYSICS OF LIPIDS

Temperature and ionic strength dependent light scattering of DMPG dispersions

Karin A. Riske [a], Mário J. Politi [b], Wayne F. Reed [c], M. Teresa Lamy-Freund [a,*]

[a] *Institute of Physics, Universidade de São Paulo, CP 66318, CEP 05315-970, São Paulo, SP, Brazil*
[b] *Institute of Chemistry, Universidade de São Paulo, São Paulo, SP, Brazil*
[c] *Department of Physics, Tulane University, New Orleans, LA, USA*

Received 4 June 1997; received in revised form 14 July 1997; accepted 14 July 1997

Abstract

The temperature dependence of the intensity of light scattered by aqueous dispersions of the anionic lipid DMPG (dimyristoyl phosphatidylglycerol) was studied at different ionic strengths. The lipid main transition, gel-liquid crystal, is clearly detected by a sharp decrease in light scattering. As expected, the temperature of the main transition (T_m) was found to increase with the increase of the ionic strength. For low ionic strength, a DMPG second temperature transition, termed the 'post-transition', can be monitored by both an increase in light scattering and a decrease in conductivity. Zimm plot analysis indicates that below T_m the liposomes tend to aggregate, and show a negative second virial coefficient A_2, and particles of large molecular weight. At the main phase transition, parallel to the decrease in light scattering, there is an increase in the sample conductivity, A_2 becomes positive and the particle molecular weight decreases, indicating that the vesicles become disaggregated. Moreover, at the post-transition (T_{post}) A_2 becomes very small, perhaps slightly negative, and the molecular weight increases again. Both the main and the post transitions were found to be reversible. In contrast to the main transition, the post-transition could not be detected by spin labels placed either at the membrane surface, or in the bilayer core. While the mechanism of increased ionization at T_m could be related to the melting of the hydrocarbon chains, the mechanism for the possible counterions recondensation at T_{post} is far less clear. © 1997 Elsevier Science Ireland Ltd.

Keywords: DMPG; Light scattering; Ionic strength; Phase transition; Surface ionization

1. Introduction

Although the thermotropic properties of charged lipids in aqueous suspensions has been extensively studied, their complex behavior has

* Corresponding author. Tel: + 55 11 8186829; fax: + 55 11 8134334; e-mail: mtfreund@fge.if.usp.br

PII S0009-3084(97)00058-3

not been fully characterized. DMPG (dimyristoyl phosphatidylglycerol), in particular, has been found to present different thermal phases depending on the lipid concentration, the sample pH, ionic strength, and time and temperature of incubation (Cevc et al., 1981; Epand and Hui, 1986; Gershfeld et al., 1986; Salonen et al., 1989; Epand et al., 1992; Kodama et al., 1993; Heimburg and Biltonen, 1994; Zhang et al., 1997). Heimburg and Biltonen (1994) observed a complex profile for the variation of the heat capacity of DMPG dispersions with temperature. For DMPG at concentrations between 10 and 150 mM, in low ionic strength (2 mM phosphate buffer and 1 mM EDTA), an intermediate thermal phase was described, called a large main transition region, characterized by high viscosity and low turbidity. Those results, together with electron microscopy, were discussed in terms of a long range order in the lipid dispersion. That same intermediate state had been seen before (Salonen et al., 1989) by DSC (differential scanning calorimetry), and was shown to be highly dependent on the solution ionic strength, and said to be limited by the main lipid transition and a second thermal transition, termed the 'post-transition'.

The present work investigates the different thermotropic states of freshly prepared DMPG, for different ionic strengths, mainly by light scattering. Zimm plot analysis of light scattering data showed that there is a net repulsion among the liposomes in the intermediate phase, accompanied by a measurable increase in the sample conductivity. A tentative, qualitative rationalization based on the Gouy–Chapman–Stern electrostatic double layer theory is discussed (see references in McLaughlin, 1977), which considers different Na^+–PG^- association constants in the gel and liquid crystal phases.

2. Materials and methods

2.1. Materials

The sodium salt of the phospholipids, DMPG (1,2-dimyristoyl-*sn*-glycero-3-phosphoglycerol) and DMPC (1,2-dimyristoyl-*sn*-glycero-3-phosphocholine), and the spin labels 5- and 12-PCSL (1-palmitoyl-2-[5- or 12- doxyl stearoyl]-*sn*-glycero-3-phosphocholine) were obtained from Avanti Polar Lipids (Birmingham, AL). SSL (stearamide spin label) was a gift from S. Schreier laboratory, at the University of São Paulo. The buffer used was 10 mM Hepes (4-(2-hydroxyethyl)-1-piperizineethanesulfonic acid) at pH 7.4. All reagents were used without further purification. Deionized water double distilled was used throughout.

2.2. Lipid dispersion preparation

A lipid film was formed from a chloroform solution of lipids, dried under a stream of N_2 and left under vacuum for a minimum of 5 h, to remove all traces of the organic solvent. Liposomes were prepared by the addition of the desired buffer or water solution, with or without added salt, followed by vortexing above the phase transition temperature. For the ESR measurements spin label solutions in chloroform were dried with the lipids, to the final concentration 1 mol% of spin label.

2.3. 90° Light scattering

A fluorimeter Hitachi F-3010 at a wavelength of 280 nm was used. The temperature was maintained with an external water bath Forma Scientific 2006, and measured with a Fluke 51 K/J thermometer placed inside the cuvette. After achieving the desired temperature, the sample was left for at least 5 min at each temperature before the measurement was done.

2.4. Multi-angle static light scattering

Static light scattering (SLS) measurements were made with a Wyatt Technology Dawn-F DSP light scattering photometer (Sta. Barbara, CA). To allow the scattering to be measured simultaneously from 18 angles, ranging from 26 to 145°, 25 mm diameter scintillation vials were used. Data was transferred via an RS-232c line to a microcomputer. One of the authors (WFR) wrote software for data acquisition and analysis.

Raw scattering voltages at each angle scattering vector $\boldsymbol{q}$, $V(\boldsymbol{q})$, were transformed to absolute Rayleigh ratios $I(\boldsymbol{q})$ according to

$$I(\boldsymbol{q}) = \frac{V(\boldsymbol{q}) - V_s(\boldsymbol{q})}{V_a(\boldsymbol{q}_r) - V_d(\boldsymbol{q}_r)} N(\boldsymbol{q}) I_a F \quad (1)$$

where $V_s(\boldsymbol{q})$ is the solvent scattering voltage at $\boldsymbol{q}$, $V_a(\boldsymbol{q}_r)$ is the voltage at a reference wavevector $\boldsymbol{q}_r$ (here taken as that corresponding to $\theta = 90°$) of the absolute calibration solvent, which in this case was toluene, with a known absolute Rayleigh scattering ratio for $\lambda = 633$ nm at $T = 25°C$ of $I_a = 1.408 \times 10^{-5}$ cm^{-1}. $V_d(\boldsymbol{q}_r)$ is the photodetector dark count at the reference wavevector. F is a geometrical correction factor which, for upright, cylindrical cells amounts to the square of the ratio of the refractive index of the sample's solvent to that of toluene, divided by the total Fresnel reflection losses at the glass–solvent interface. The scattering vector $\boldsymbol{q}$ has its usual definition as

$$\boldsymbol{q} = (4\pi n/\lambda) \sin(\theta/2) \quad (2)$$

where n is the index of refraction of the solvent, λ is the vacuum wavelength of the laser and θ is the scattering angle. $N(\boldsymbol{q})$ is the normalization factor for each photodiode which is computed according to

$$N(\boldsymbol{q}) = \frac{V_n(\boldsymbol{q}) - V_s(\boldsymbol{q}_r)}{V_n(\boldsymbol{q}) - V_s(\boldsymbol{q})} \quad (3)$$

where $V_n(\boldsymbol{q}_r)$ is the scattering voltage of the normalization solution in the sample solvent at the reference wavevector. The normalization solution is composed of an isotropic scatterer in the sample solvent. In this case a solution of dextran of weight average molecular weight $M_w = 15\,000$ at 15 mg ml^{-1} in water was used as the normalizing solution.

The standard Zimm single contact approximation for a single component system (Zimm, 1948) was used for analyzing the total Rayleigh ratios

$$\frac{Kc}{I(\boldsymbol{q})} = \frac{1}{M_w P(\boldsymbol{q})} + 2A_2 c Q(\boldsymbol{q}) \quad (4)$$

where M_w is the weight average molecular weight of the scatterer, and $P(\boldsymbol{q})$ is the particle form factor, which, in the limit $\boldsymbol{q}^2 < R_g^2 > < 1$ is approximated, for particles of any shape, by

$$P(\boldsymbol{q}) \sim 1 - \frac{\boldsymbol{q}^2 < R_g^2 >_z}{3} \quad (5)$$

Here, $< R_g^2 >_z$ is the z-averaged mean square radius of gyration. K is an optical constant, given for vertically polarized light as

$$K = \frac{4\pi^2 n^2 (\partial n/\partial c)^2}{N_A \lambda^4} \quad (6)$$

$Q(\boldsymbol{q})$ depends on both particle form factor and interparticle interactions. In the current case of fairly small particles ($\boldsymbol{q}^2 R_g^2 < 1$) in dilute solution, we make the approximation that $Q(\boldsymbol{q}) = 1$.

N_A is Avogadro's number and $\partial n/\partial c$ is the refractive index increment of the solution per unit mass concentration increase of lipid. An average value of 0.12 ml g^{-1} was used here for DMPG.

2.5. ESR spectroscopy

ESR measurements were performed in a Bruker ER 200D-SRC spectrometer interfaced with an IBM-PC like computer for spectrum digitalization. A field modulation amplitude of 0.08 mT and microwave power of 10 mW were used. The temperature was controlled to about 0.5° with a Bruker B-ST 100/700 variable temperature device. The temperature was always monitored with a Fluke 51 K/J thermometer. For the measurement of the spectrum parameters, A_{max}, the outer hyperfine splitting, and the linewidth of the low field line ($m_I = +1$) the *ORIGIN* software (MicroCal Software, MA) was used.

2.6. Refractive index

Refractive index was measured with a Carl Zeiss Abbe refractometer, equipped with a jacketed cell. Water was circulated to the cell from a constant temperature water bath Forma Scientific 2006, and temperature was measured with a Fluke 51 K/J thermometer in contact with the sample. A sodium lamp ($\lambda \approx 590$ nm) was used.

2.7. Conductivity

A standard platinum electrode (1 cm^2) with a conductivimeter Digimed CD-20 Brazil was used.

3. Results

3.1. General light scattering trends

The DMPG main thermal transition can be clearly monitored by the sharp decrease in light scattering. Fig. 1 shows the temperature dependence of the light scattered at $\theta = 90°$ by two samples (the trend of the light scattering is the same for all angles in the measurable range): DMPG liposomes at relatively high ionic strength (100 mM NaCl) and zwitterionic DMPC liposomes. Both samples display a sharp drop around 22.5°C, indicating their gel–liquid crystal transition temperature (T_m).

However, DMPG at low ionic strength, 10 mM Hepes buffer only, shows a light scattering pattern rather different from those discussed above. The main transition continues to be clearly seen, and there is another transition (called here post-transition), which appears at around 35°C (Fig. 2). The DMPG post-transition has been seen before by light scattering (Heimburg and Biltonen, 1994), and DSC (Salonen et al., 1989), but, contrary to the main transition, it has not been well characterized. Fig. 2 shows that both the main and the post transitions are reversible. However, whereas the temperature of the main transition, T_m, measured by light scattering, does not change after 48 h of incubating the sample at 30°C, the post-transition temperature, T_{post}, decreases in time. It is important to note that for DMPG at low ionic strength the ratio between the intensity of the light scattered before and after T_m is much higher (about 4-fold, in Fig. 2) than that observed at high ionic strength (Fig. 1).

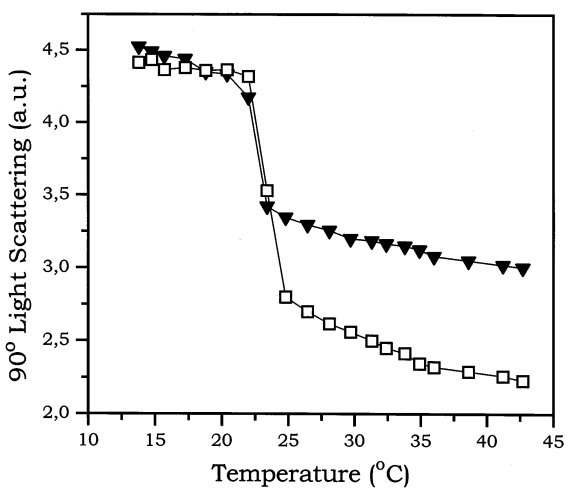

Fig. 1. Temperature dependence of 90° light scattering of dispersions of 10 mM DMPG + 100 mM NaCl (▼) and 10 mM DMPC (□) in 10 mM Hepes buffer pH 7.4.

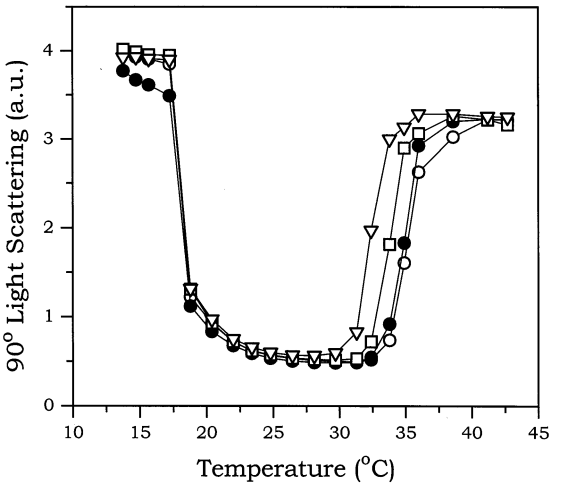

Fig. 2. Temperature dependence of 90° light scattering of 10 mM DMPG in 10 mM Hepes pH 7.4, freshly prepared, temperature up (○) and temperature down (●), after 1 day (□) and after two days (▽) incubation at 35°C.

For some liposomes, the sharp decrease in turbidity at the gel–liquid crystal transition has been attributed to a change in the increment of refractive index (dn/dc), related to the known vesicle swelling and corresponding decrease in the bilayer density and thickness at the phase transition (Yi and MacDonald, 1973; Disalvo, 1991). Fig. 3 shows the temperature dependence of dn/dc for two DMPG samples: in the absence and in the presence of 100 mM NaCl. For the high ionic strength sample the observed variation of turbidity at the main transition (around 1.3, Fig. 1) could be related to a change in the refractive index n or to the square of dn/dc, as it appears in the Rayleigh scattering approximation (the ratio of $(dn/dc)^2$ below and above T_m is around 1.2, Fig. 3). For the low ionic strength sample no significant variation of the refractive index increment could be detected at the transition tempera-

ture (18°C). Even considering dn/dc over the whole range of temperature (from 10 to 40°C $(dn/dc)^2$ changes by a factor of 1.4), its variation cannot explain the drop in light scattering at T_m, indicating that the large change in turbidity at the phase transition must have a different origin.

The transition temperature of ionized DMPG is known to increase with the increase of the ionic strength (Träuble et al., 1976), reaching the value of 29°C at about 2 M NaCl (Cevc et al., 1980). The shift in T_m can be attributed to the screening of the DMPG negative charges by the counterions present in solution. The decrease of the surface potential would increase the stability of the gel state more than that of the fluid state, leading to a higher phase transition temperature (Jähnig, 1976; Träuble et al., 1976; Cevc et al., 1980). The dependence of both T_m and T_{post} on the ionic strength is clearly seen by light scattering (Fig. 4). In distilled water DMPG displays a gradual decrease in turbidity with temperature, paralleling the results obtained with DSC (Epand and Hui, 1986), which showed that the DMPG main thermal transition was very broad. That result, together with freeze-fracture electron microscopy, led the authors to suggest that, at very low ionic strength, DMPG could destabilize bilayers and form smaller particles due to the strong repulsion between the charged layers (Epand and Hui, 1986).

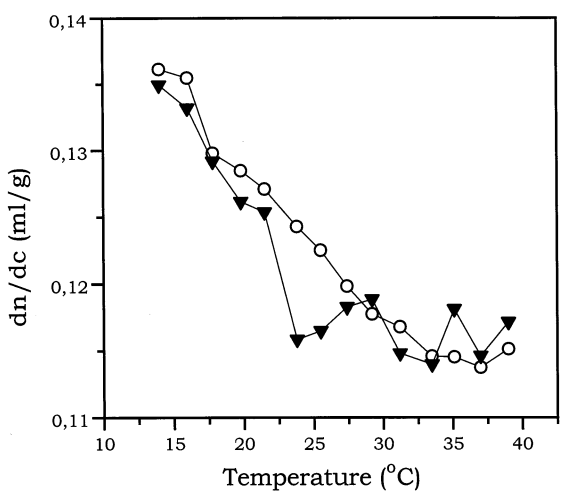

Fig. 3. Temperature dependence of the refractive index increment (dn/dc) of dispersions of DMPG in 10 mM Hepes pH 7.4 in the absence (○) and in the presence of 100 mM NaCl (▼). DMPG concentrations from 1 to 70 mM.

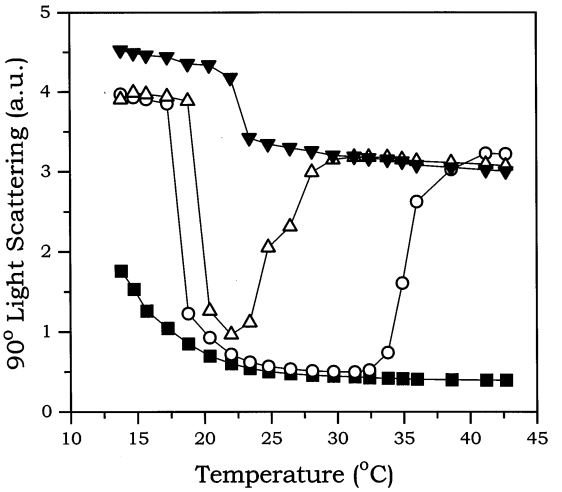

Fig. 4. Temperature dependence of 90° light scattering of dispersions of 10 mM DMPG in distilled water (■) and in 10 mM Hepes pH 7.4 with no added salt (○); + 10 mM (Δ); and + 100 mM NaCl (▼).

The sharp decrease in light scattering at the phase transition, allows the measurement of rather accurate T_m values for DMPG at the conditions used here (Table 1). In contrast to the main transition, the post-transition temperature decreases as the ionic strength increases, and disappears completely at 100 mM NaCl, as seen before (Fig. 1). Below T_m and above T_{post} the samples are visibly cloudy. In distilled water DMPG dispersions are transparent for all temperatures studied here, as opposed to the high ionic sample (100 mM NaCl) which is cloudy at all temperatures. Interestingly, the high salt and dis-

Table 1
Transition temperatures of DMPG dispersions, measured by light scattering, for different lipid concentrations in different ionic strengths

Sample	T_m (°C)	T_{post} (°C)
10 mM DMPG in 10 mM Hepes	18.0	35.0
+ 10 mM NaCl	19.5	26.0
+ 100 mM NaCl	22.5	—
50 mM DMPG in 10 mM Hepes	19.5	26.0

tilled water samples provide well defined upper and lower limits, between which the scattering of all other samples varied.

Similar to the results obtained with DSC (Heimburg and Biltonen, 1994), light scattering also detects an increase in T_m and a decrease in T_{post} with the increase of the DMPG concentration (Table 1).

Results comparable to those obtained with 10 mM NaCl were obtained with the same concentration of KCl. The T_m values found in the presence of the two cation species were very similar, but T_{post} for K^+ was lower, about 22.5°C, indicating some ion specific effect. The presence of 10 mM of Na_2SO_4 resulted in an increase in T_m ($T_m \sim 20$°C) and decrease in T_{post} ($T_{post} \sim 22$°C), possibly due to its higher ionic strength as compared with NaCl. Further studies on the effect of different ions on T_m and T_{post} could possibly indicate some correlation between the change in the phase transition temperatures and the ions so-called water 'structure maker' or 'structure breaker' (Toko and Yamafuji, 1980; Conway, 1981; Kraayenhof et al., 1996). It is important to note that similar results were obtained with phosphate buffer, indicating that there is no specific effect of the Hepes buffer.

All the thermal transitions shown here, measured by changes in the sample light scattering, were found reversible, and, for a given temperature, they were found stable for at least a few hours. In terms of the overall stability and reproducibility of the DMPG vesicles, it is important to make the following observations. The method of preparing the DMPG vesicles does not lead to a unique dispersion for each preparation. There can be significant batch-to-batch variation in the vesicles in terms of M_w, $< R_g >_z$ and polydispersity, as will be discussed below, although the results obtained in Figs. 1 and 2 and Fig. 4 were rather reproducible. Furthermore, the vesicles are not stable against aggregation over a time scale of weeks. Hence, the vesicles can only be considered as in a metastable state. The temperature cycling experiments, however, were performed over a scale of hours, which is very short compared to the long term scale of vesicle instability, so that the vesicles were in equilibrium over the interval of the reversibility experiments.

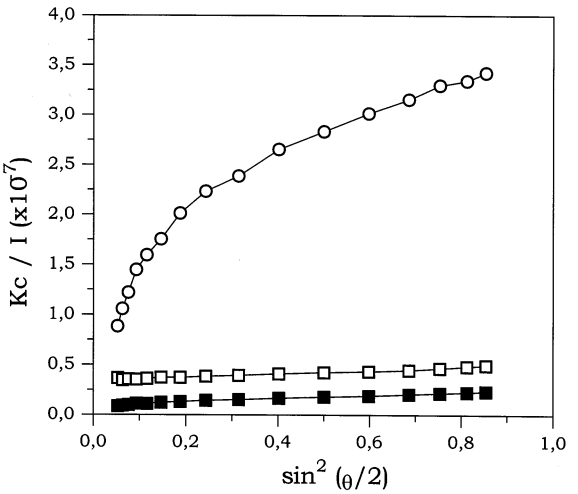

Fig. 5. Kc/I (Eq. (4)) as a function of $\sin^2(\theta/2)$ for 1.0 mM DMPG in 10 mM Hepes pH 7.4 at $T = 15$°C (■); 23°C (○); and 40°C (□).

3.2. Light scattering results on vesicle mass and interactions

The light scattered at different angles displays the same pattern as that observed at 90°. Namely, the plots of Kc/I vs. $\sin^2(\theta/2)$ in Fig. 5 show that, between T_m and T_{post}, the light scattered at all angles, by the low ionic strength sample, was significantly less intense than that scattered below T_m and above T_{post}. Table 2 shows typical Zimm plot results for a particular preparation of DMPG liposomes in 10 mM Hepes buffer, at three temperatures: before the main transition, between the two transitions and after the post transition.

There was considerable polydispersity, as could be detected by the strong scattering at low angles, and only angles from 45° and higher were used. There was significant variation in the values of the

Table 2
Typical Zimm plot results for a DMPG dispersion in 10 mM Hepes buffer, for three temperature regions: below T_m (13°C), between T_m and T_{post} (22°C), and above T_{post} (40°C)

T (°C)	M_w (MDa)	A_2 (cm·mol per g^2)	R_g (nm)
13	60	-2.0×10^{-6}	65
22	15	30×10^{-6}	80
40	40	1.0×10^{-6}	60

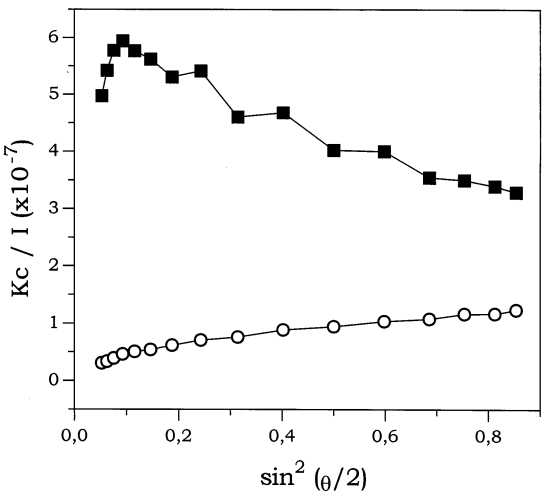

Fig. 6. Comparison of Kc/I (Eq. (4)) as a function of $\sin^2(\theta/2)$ for 1.0 mM DMPG in distilled water (■) and in 10 mM Hepes pH 7.4 (○).

results when different preparations were measured, with M_w, R_g and A_2 changing up to 100%. However, the overall trends were always the same. For a given preparation, below T_m the mass is high, and A_2 is very low and negative, indicating some net attraction, and hence aggregation of the liposomes. After T_m, A_2 becomes positive and large, indicating net repulsion, and the mass drops significantly, while R_g increases somewhat. For higher temperatures, after the post-transition, A_2 becomes extremely small or even slightly negative, indicating a considerable decrease in the repulsive force between the liposomes, which parallels an increase in M_w. Apparently, between the two temperature transitions, a repulsive force between the charged liposomes dominate over the van der Waals attraction. This could be explained by an increase in the vesicles surface charge between T_m and T_{post}, consistent with the increase in reduced solution conductivity in this range, as will be shown later.

3.3. Light scattering shows strong intervesicular correlations in the absence of added salt

DMPG dispersions in solutions with no added salt display scattering behavior characteristic of strongly interacting, electrically charged particles. Fig. 6 compares the Kc/I versus $\sin^2(\theta/2)$ for 1 mM DMPG in water with no added salt and in 10 mM Hepes added at 25°C. The fact that Kc/I has a negative slope in the case of pure water indicates the strong interparticle correlation which occur. In 10 mM Hepes, these strong interactions are screened out by the mobile electrolytes in the Hepes, and Kc/I shows the positive slope typical of weakly interacting particles. In short, the total scattered intensity can be approximated by $I(\boldsymbol{q}) \propto S(\boldsymbol{q})P(\boldsymbol{q})$, where $S(\boldsymbol{q})$ is the interparticle structure factor, given by

$$S(\boldsymbol{q}) = 1 + 4\pi N \int_0^\infty (1 - g(r))\, \mathrm{d}^3 r \tag{7}$$

$g(r)$ being the interparticle correlation function, given by

$$g(r) = \exp(-U(r)/kT) \tag{8}$$

where $U(r)$ is the potential energy between two particles at a separation r from each other. $P(\boldsymbol{q})$ is the particle form factor appearing in Eq. (4). When interparticle interactions are relatively weak, such as when added salt is present, $S(\boldsymbol{q})$ is essentially a $\boldsymbol{q}$-independent constant and the angular dependence of $I(\boldsymbol{q})$ is determined by $P(\boldsymbol{q})$, the particle form or shape factor. For the vesicles in this work the approximate Eq. (4) applies fairly well, and a linear increase of $1/I(\boldsymbol{q})$ is seen when screening is present, such as for the case of DMPG in Hepes shown in Fig. 6. When repulsive correlations are strong, however, such as in the absence of added salt, $S(\boldsymbol{q})$ is very small at $\boldsymbol{q} = 0$, increases to a maximum value and then decreases. The inverse of $I(\boldsymbol{q})$ is hence a decreasing function, as seen in the pure water case of DMPG in Fig. 6. The peak in this case is apparently off the high end of the $\boldsymbol{q}^2$ (or $\sin^2(\theta/2)$) plot. In fact, as has been demonstrated (Krause et al., 1989; Wang and Bloomfield, 1991; Maier et al., 1992) the $\boldsymbol{q}$ for which the peak of $S(\boldsymbol{q})$ occurs, termed $\boldsymbol{q}_p$, is given, for very dilute particles of any shape by

$$\boldsymbol{q}_p = 2\pi[C_p N_A/M]^{1/3} \tag{9}$$

where C_p is the concentration in g ml^{-1} and M is the molar mass. For $C_p = 1$ mg ml^{-1} and $M \sim 10^7$ $\boldsymbol{q}_p$ is 2.45×10^5 cm^{-1}. This is close to the maximum measurable $\boldsymbol{q}$ of the multi-angle laser

light scattering system, which is $q = 2.5 \times 10^5$ cm^{-1}, at $\theta = 145°$. Given that such light scattering maxima are usually quite broad in q, and that there is significant vesicle polydispersity, it would presumably take more dilute solutions to unambiguously identify and measure q_p.

Such scattering peaks, although reminiscent of Bragg peaks in X-ray diffraction cases, are nonetheless quite broad, and have been recently interpreted in terms of liquid-like correlations (Li and Reed, 1991; Morfin et al., 1994; Norwood et al., 1996). There is a fair, but not unanimous consensus, that such scattering behavior reflects dynamic correlations between particles and in no way implies a static, long range ordering of particles. In fact, evidence was recently found that the scattering peaks for such particles remain the same even under high shear flow conditions, further suggesting that no long-range or static structuring is involved (Reed, 1994). A damped, quasi-periodic potential for $U(r)$ in Eq. (8) was recently proposed (Norwood et al., 1996), which gives a good account of the observed scattering. Therefore, there is no reason to suspect any type of long-range ordering in any of the DMPG dispersions.

3.4. Spin label ESR

As is well known, the gel–liquid crystal transition of lipid vesicles, related to an increase in the order/mobility of the hydrocarbon chains, can be monitored by spin labels placed at different positions in the bilayer. Fig. 7 shows the dependence of some EPR parameters with the temperature, using two different labels which give information about different micro-regions of the bilayer, incorporated in DMPG dispersions. The parameters were chosen considering their accuracy and reproducibility at all temperatures, and their sensitivity to temperature and ionic strength variation. The outer hyperfine splitting A_{max} and the linewidth of the low field line ($m_I = +1$) are the empirical parameters used here. In general, an increase in both the linewidth and A_{max} is associated with an increase of the label environment viscosity or packing. Although 12-PCSL in membranes is known to present a large vertical fluctuation (Godici and Landsberger, 1974; Yin et al., 1988), it monitors, on average, a deeper position in the bilayer core than 5-PCSL (Biaggi et al., 1996). The lipid main phase transition is better followed by a spin label down in the bilayer like 12-PCSL, than by 5-PCSL, near the interface. As expected, the two labels show that the main phase transition temperature, T_m, increases with the increase of the sample ionic strength. Although the phase transitions monitored by the spin labels are much less sharp (even for 12-PCSL) than those measured by light scattering, the T_m values are rather similar. However, it is noteworthy that, opposite to the main transition, the post-transition could not be detected by the spin labels used here. Similar results were obtained with SSL (not shown), which monitors the membrane interface.

It has been suggested before that DMPG in pure water produces small discs or shells rather than large bilayer vesicles (Epand and Hui, 1986). However, it is important to note that although the light scattering pattern of DMPG in water is very different from that in Hepes buffer, the hydrocarbon chain packing of the two samples are rather similar for low (10°C) and high (above 25°C) temperatures, as indicated by the ESR parameters of spin labels intercalated in the aggregates (Fig. 7). Moreover, the ESR spectra yielded by 5- and 12-PCSL incorporated in soya lecithin vesicles at 10°C, which are in the liquid crystal state, or in different types of micelles, at the same temperature, are typical of a much more mobile environment (results not shown) than those obtained with DMPG, in Hepes or pure water solution, at 10°C. Therefore, strongly suggesting that, even in pure water, DMPG is organized in bilayers, with highly packed hydrocarbon chains at low temperatures. The light scattering and spin labeling results shown here, together with differential scanning calorimetry and freeze-fracture electron microscopy (Epand and Hui, 1986), would be in accord with the formation of small aggregates which would still keep some bilayer structure, but displaying no sharp phase transition.

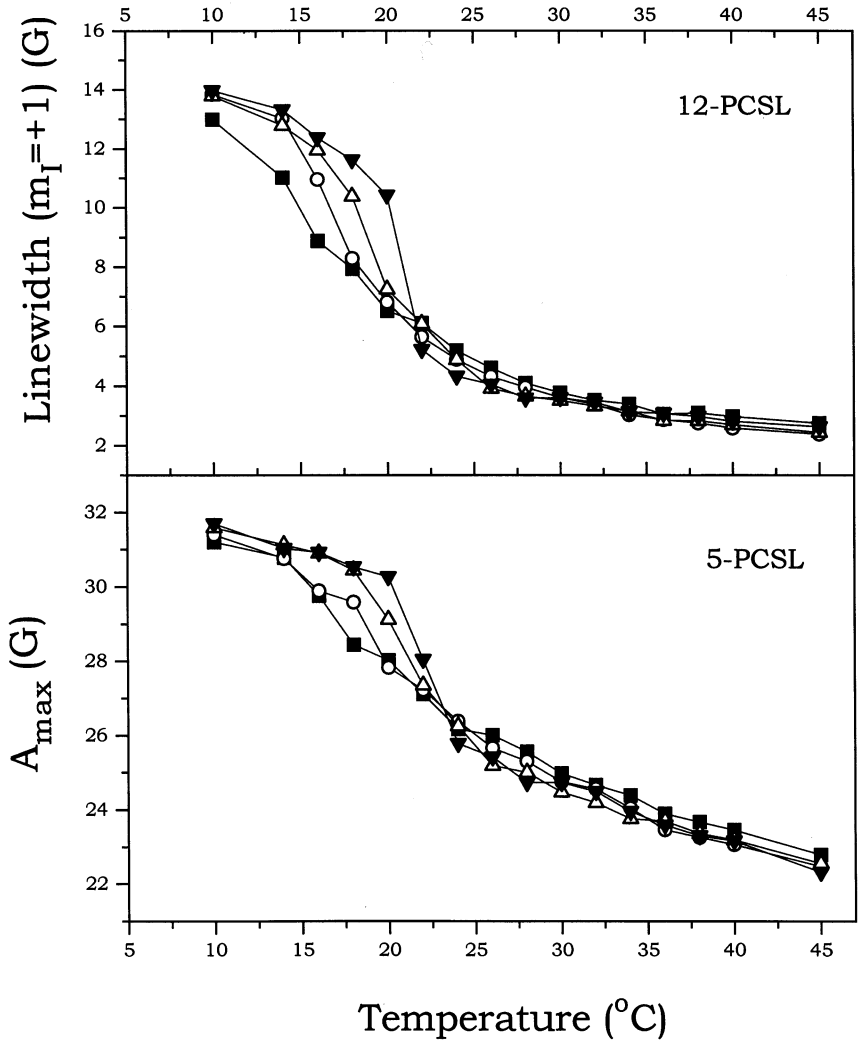

Fig. 7. Measured parameters from ESR spectra of 1 mol% of 12-PCSL and 5-PCSL incorporated in 10 mM DMPG in distilled water (■) and in 10 mM Hepes pH 7.4 with no added salt (○), + 10 mM (Δ) and + 100 mM NaCl (▼).

3.5. Conductivity

To further investigate the temperature dependent ionization window suggested by the light scattering experiments, conductimetric measurements were made for 10 mM DMPG dispersion in Hepes buffer. The results are shown in Fig. 8 as a 'reduced' or 'excess conductivity', defined as the difference in conductivity between the DMPG and pure solvent samples, divided by pure solvent conductivity at each temperature. This reduced conductivity eliminates the effect of mere increased mobility on conductivity with increasing temperature and should reflect changes in concentrations of mobile ions, related to changes in DMPG headgroup ionization. Though the temperature transitions are not sharply indicated, it can be seen that below T_m and above T_{post} the sample conductivity is rather low, as compared to that in between the two transitions. Those results corroborate the discussion made above, in the sense that both the vesicle surface charge and the

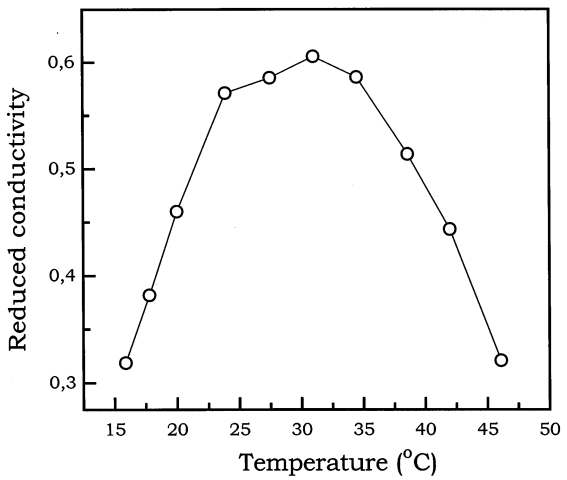

Fig. 8. Reduced conductivity as a function of temperature for 10 mM DMPG in 10 mM Hepes pH 7.4.

related ion concentration in the bulk are higher between the two phase transitions.

4. Discussion

The experimental results presented here suggest that, below T_m, DMPG liposomes have a net attraction, since A_2 is negative. At T_m, for relatively low ionic strength (i.e. below 100 mM), the melting of the hydrocarbon chains, which is known to cause an increase in the area per lipid headgroup, leads to a sharp decrease in the light scattered by the lipid dispersion (scattered intensity typically falls to less than 1/4 its level before the transition). This decrease in scattering is much too large to be accounted for by the relatively modest change in dn/dc (Fig. 3), and is related to a significant decrease in the mass of vesicular aggregates. Moreover, after T_m and below T_{post}, a strong positive A_2 is measured, which indicates a net repulsion among the vesicles, and conductivity increases throughout this range. R_g also appears to increase at the melting transition. The simplest explanation is that below T_m the vesicles are aggregated in clusters, which then fall apart due to a net repulsion above T_m. This net repulsion is likely to be gained by an increased ionization of the vesicles surface, hence increasing its potential. Above the post-transition temperature, T_{post}, the dispersion scatters as strongly as before T_m, and a large M_w is again measured, with an A_2 value close to zero (either weakly negative or positive). The reduced conductivity also decreases. A possible interpretation here is that there is a recondensation of counterions on the vesicle surface, which lowers the potential and leads to a net attraction, and re-aggregation of the vesicles.

The interpretation that the vesicles are in a disaggregated state in the T_m to T_{post} range is consistent with the increase in viscosity observed by Heimburg and Biltonen (1994) between T_m and T_{post}. Qualitatively, this is rationalized as follows: The total solution viscosity η is given by (Tanford, 1961)

$$\eta = \eta_0(1 + [\eta]C_p + \beta[\eta]^2C_p^2 + \cdots) \tag{10}$$

where η_0 is the viscosity of the pure solvent, $[\eta]$ is the intrinsic viscosity of the particle, C_p is the particle concentration in g cm^{-3}, and β is a function of two body hydrodynamic interactions between particles. Since the experiments in this work are in quite dilute solutions it suffices to consider the first two terms in parentheses above. For spheres, intrinsic viscosity is given by

$$[\eta] = \frac{2.5N_AV_H}{M} \tag{11}$$

where V_H is the hydrodynamic volume of the particle. For a unilamellar vesicle the radius of gyration is nearly equal to the hydrodynamic radius so that Eq. (11) can be approximated for dilute solutions as

$$\eta = \eta_0\left(\frac{1 + 10\pi N_AR_g^3}{3M}C_p\right) \tag{12}$$

From Table 2 we see that, between the two phase transitions, R_g remains roughly the same, but M decreases. Since C_p, the total surfactant concentration (g ml^{-1}), does not change, solution viscosity should increase when vesicles disaggregate with only minor change in R_g in the T_m to T_{post} regime.

The interaction between two charged vesicles can be described by considering the balance of four forces: the electrostatic double layer repulsion (which is actually entropic (Israelachvili,

1992)); the attractive van der Waals force and; at very short distance, the repulsive hydration and steric forces (LeNeveu et al., 1977; Parsegian et al., 1991).

Focusing only on the standard electrostatic double layer model, considering H^+ and Na^+ association with the phosphate groups at the surface of DMPG bilayers, the changes in light scattering observed at the main thermal phase transition could be related with the known change in the area per lipid headgroup at T_m, and its effect on the degree of phosphate dissociation, α, the vesicle surface potential Ψ_0, hence, in the interaction between vesicles (Israelachvili, 1992). Theoretical values for α and Ψ_0 were calculated solving numerically the equation for α (Helm et al., 1986), in the high potential approximation, considering uniformly charged planes in the Gouy–Chapman–Stern model, ionic strength 4 mM (corresponding to DMPG in 10 mM Hepes buffer, pH 7.4), and 48 and 60 Å^2, for the areas per lipid headgroup (f) in the gel and liquid crystal phases, respectively (Marsh, 1974; Watts et al., 1981). The H^+–PG^- association constant used was 15.8 M^{-1} (Toko and Yamafuji, 1980; or calculated from Watts et al., 1978). The choice of Na^+–PG^- association constant, K_{Na}, is more difficult, as some authors do not consider the binding of monovalent cations to phosphatidylglycerol (Träuble and Eibl, 1974; Träuble et al., 1976; Cevc et al., 1980; Copeland and Andersen, 1982), whereas there are several different calculations of Na^+–PG^- in the literature (Eisenberg et al., 1979; Loosley-Millman et al., 1982; Lakhdar-Ghazal et al., 1983; Helm et al., 1986; Lakhdar-Ghazal and Tocanne, 1988; Tocanne and Tessié, 1990), with K_{Na} values varying in a wide range, from 0.1 to 1 M^{-1}. The dependence of the calculated surface potential with the Na^+–PG^- association constant is plotted in Fig. 9. It is important to point out that large variations of K_H have negligible effect on α or Ψ_0, in the conditions used here. Moreover, considering only the PG^-–H^+ binding, α does not change significantly for the different conditions used here (different areas per headgroup, and ionic strength), as expected for a group in a pH far from its pK value.

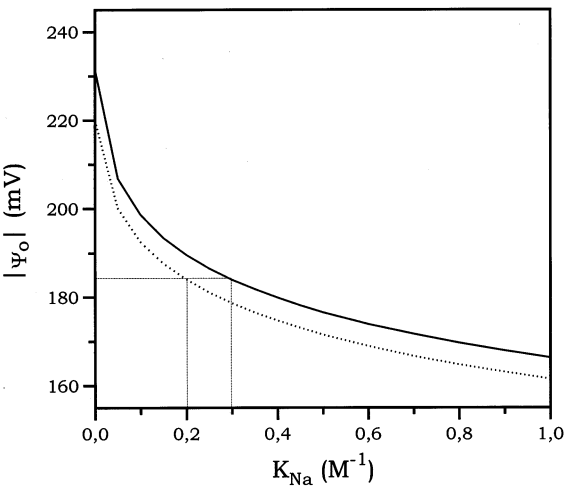

Fig. 9. Dependence of the calculated surface potential (Gouy–Chapman–Stern model) with the Na^+–PG^- association constant, K_{Na}. The areas per lipid headgroup were 48 Å^2 (——) and 60 Å^2 (···), corresponding to the gel and liquid crystal phases, respectively. Ionic strength was 4 mM and $K_H = 15.8$ M^{-1}.

Fig. 9 shows that assuming the same K_{Na} for the gel and liquid crystal phases, independent of its value, the magnitude of the surface potential is always lower after T_m ($f = 60$ Å^2) than before ($f = 48$ Å^2). That would not be in accord with the experimental data shown here, which indicate that there is an increase in the vesicles repulsion on the main thermal transition. Therefore, it is necessary to assume that the more fluid DMPG phase has a lower Na^+ binding constant than the gel phase. For instance, if K_{Na} is assumed to be 0.3 M^{-1} for the gel phase[1], the K_{Na} value for the liquid crystal phase would have to be lower than 0.2 M^{-1}, to result in a more negative Ψ_0 after T_m (see Fig. 9).

Also important to be considered is the conductivity experimental data (Fig. 8), showing that there is an increase in the amount of ions in solution after T_m. The model used here shows that for $K_{Na} = 0$ M^{-1} there is no significant increase in the degree of PG dissociation upon the gel–liquid

[1] it is interesting to note that considering $K_{Na} = 0.3$ M^{-1}, and the Gouy–Chapman–Stern model, it is possible to calculate a surface potential very similar to that measured by Cevc et al. (1980) for DMPG in 100 mM salt (99 mV), in the gel phase

crystal transition. The variation in α increases with the increase of K_{Na} (results not shown). For instance, for $K_{Na} = 0.3\ M^{-1}$ for the two phases, there is a 12% increase in a value upon the transition, with the corresponding increase in the amount of ions in solution. If it is assumed K_{Na} values of 0.3 and 0.1 M^{-1}, for the gel and liquid crystal phases, respectively, the more fluid phase would be 48% more ionized than the gel state. About the possible dependence of K_{Na} on the area per lipid headgroup, it could be speculated that the amount of bound counterion is a function of the packing of the lipids, water organization and/or local dielectric constant dependent on temperature or surface undulations. Although in a different system, it is interesting to point out that Loosley-Millman et al. (1982) suggested that the binding of Na^+ ions to negatively charged bilayers might increase as the bilayers are pushed together, possibly related to their electric fields perturbing the conformation of neighboring polar groups.

If the above model is applied to DMPG in pure water (ionic strength 0.0025 mM and $f = 48$ Å^2), a very low degree of PG dissociation is found, $\alpha = 0.12$, in accord with experiments with DMPG monolayers (Tocanne et al., 1974; Sacré and Tocanne, 1977). However, due to the low ionic strength, even with the low vesicle surface charge, the magnitude of the surface potential is rather high, $\Psi_0 = -313$ mV, which could be responsible for a great repulsion among vesicles. That would explain the observed strong interparticle correlation effect with DMPG in water (Fig. 6), and the DSC results obtained by Epand and Hui (1986).

The mechanism that could cause the counterions recondensation at T_{post}, for DMPG in Hepes buffer, is more difficult to be understood, as the possible post-transition structural changes are unknown, and could not be monitored by spin labels placed in the lipid bilayer.

Very simple considerations on the low scattering window between T_m and T_{post} have been presented here. We wanted to point out that it is necessary to have a lower K_{Na} value in that temperature region in order to obtain a certain minimum increase in surface potential, which would cause the aggregated vesicles to repel strongly enough to disaggregate. However, in order to get a negative value for A_2, there must be attractive intervesicle forces. The origin of these, if any exist besides the standard van der Waals dipole forces, is not clear. An alternative to the above hypothesis would be that at T_m the attractive forces are lost and net repulsion takes over, i.e. the increase in conductivity and surface ionization does not necessarily cause the aggregated vesicles to separate, but rather the loss of attractive forces. In this alternative, above T_{post} the attractive forces reappear and the vesicles re-aggregate. On the other hand, the hydration forces could also play an important role in the inter-vesicle interactions.

Acknowledgements

This work was supported by FAPESP, CNPq and FINEP. CNPq fellowships for KAR and MTLF. (research) are acknowledged. We are grateful to Dr V.B. Henriques and to Dr C. Goldman for very helpful discussions, and to Dr S. Schreier for making the ESR spectrometer available. WFR acknowledges travel support from FAPESP and SBBq.

References

Biaggi, M.H., Pinheiro, T.J., Watts, A., Lamy-Freund, M.T., 1996. Spin label and 2H-NMR studies on the interaction of melanotropic peptides with lipid bilayers. Eur. Biophys. J. 24, 251–259.

Cevc, G., Watts, A., Marsh, D., 1980. Non-electrostatic contribution to the titration of the ordered-fluid phase transition of phosphatidylglycerol bilayers. FEBS Lett. 120 (2), 267–270.

Cevc, G., Watts, A., Marsh, D., 1981. Titration of the phase transition of phosphatidylserine bilayers membranes. Effects of pH, surface electrostatics, ion binding, and headgroup hydration. Biochemistry 20, 4955–4965.

Conway, B.E., 1981. Ionic Hydration in Chemistry and Biophysics. Elsevier, Amsterdam.

Copeland, B.R., Andersen, H.C., 1982. A theory of effects of protons and divalent cations on phase equilibria in charged bilayer membranes: Comparison with experiments. Biochemistry 21, 2811–2820.

Disalvo, E.A., 1991. Optical properties of lipid dispersions induced by permeant molecules. Chem. Phys. Lipids 59, 199–206.

Eisenberg, M., Gresalfi, T., Riccio, T., McLaughlin, S., 1979. Adsorption of monovalent cations to bilayer membranes containing negative phospholipids. Biochemistry 18, 5213–5223.

Epand, R.M., Hui, S.W., 1986. Effect of electrostatic repulsion on the morphology and thermotropic transitions of anionic phospholipids. FEBS Lett. 209 (2), 257–260.

Epand, R.M., Gabel, B., Epand, R.F., Sen, A., Hui, S.W., 1992. Formation of a new stable phase of phosphatidylglycerol. Biophys. J. 63, 327–332.

Gershfeld, N.L., Stevens Jr, W.F., Nossal, R.J., 1986. Equilibrium studies of phospholipids bilayer assembly. Faraday Discuss. Chem. Soc. 81, 19–28.

Godici, P.E., Landsberger, F.R., 1974. The dynamic structure of lipid membranes. A ^{13}C nuclear magnetic resonance study using spin labels. Biochemistry 13, 362–368.

Heimburg, T., Biltonen, R.L., 1994. Thermotropic behavior of dimyristoylphosphatidylglycerol and its interaction with cytochrome c. Biochemistry 33, 9477–9488.

Helm, C.A., Laxhuber, L., Lösche, M., Möhwald, H., 1986. Electrostatic interactions in phospholipid membranes. I: Influence of monovalent ions. Colloid Polym. Sci. 264, 46–55.

Israelachvili, J., 1992. Electrostatic forces between surfaces in liquids. In: Intermolecular and Surface Forces. Academic Press, London, pp. 213–259.

Jähnig, F., 1976. Electrostatic free energy and shift of the phase transition for charged lipid membranes. Biophys. Chem. 4, 309–318.

Kodama, M., Miyata, T., Yokoyama, T., 1993. Crystalline cylindrical structures of Na^+-bound dimyristoylphosphatidylglycerol as revealed by microcalorimetry and electron microscopy. Biochim. Biophys. Acta 1168, 243–248.

Kraayenhof, R., Sterk, G.J., Sang, H.W.W.F., Krab, K., Epand, R.M., 1996. Monovalent cations differently affect membrane surface properties and membrane curvature, as revealed by fluorescent probes and dynamic light scattering. Biochim. Biophys. Acta 1282, 293–302.

Krause, R., Maier, E.E., Deggelmann, M., Hagenbuchle, M., Schulz, S.F., Weber, R., 1989. Static light scattering by solutions of slat-free polyelectrolytes. Physica A 160, 135–147.

Lakhdar-Ghazal, F., Tichiadou, J.L., Tocanne, J.F., 1983. Effect of pH and monovalent cations on the ionization state of phosphatidylglycerol in monolayers. Eur. J. Biochem. 134, 531–537.

Lakhdar-Ghazal, F., Tocanne, J.F., 1988. Modulation of the adsorption of alkaline cations to phosphatidylglicerol by a dimannosyldiacylglycerol. Biochim. Biophys. Acta 943, 19–27.

LeNeveu, D.M., Rand, R.P., Parsegian, V.A., Gingell, D., 1977. Measurement and modification of forces between lecithin bilayers. Biophys. J. 18, 209–230.

Li, X., Reed, W.F., 1991. Polyelectrolyte properties of proteoglycan monomers. J. Chem. Phys. 94, 4568–4580.

Loosley-Millman, M.E., Rand, R.P., Parsegian, V.A., 1982. Effects of monovalent ion binding and screening on measured electrostatic forces between charged phospholipid bilayers. Biophys. J. 40, 221–232.

Maier, E.E., Krause, R., Deggelmann, M., Hagenbuchle, M., Weber, R., Fraden, S., 1992. Liquidlike order of charged rodlike particle solutions. Macromolecules 25, 1125–1133.

Marsh, D., 1974. An interaction spin label study of lateral expansion in dipalmitoyllecithin-cholesterol bilayers. Biochim. Biophys. Acta 363, 373–386.

McLaughlin, S., 1977. Electrostatic potentials at membrane–solution interfaces. Curr. Top. Membr. Transp. 9, 71–144.

Morfin, I., Reed, W.F., Rinaudo, M., Borsali, R., 1994. Further evidence of liquid-like correlations in polyelectrolyte solutions. J. Phys. II France 4, 1001–1035.

Norwood, D.P., Benmouna, M., Reed, W.F., 1996. Static light scattering from mixtures of polyelectrolytes in low ionic strength solutions. Macromolecules 29, 4293–4304.

Parsegian, V.A., Rand, R.P., Fuller, N.L., 1991. Direct osmotic stress measurements of hydration and electrostatic double-layer forces between bilayers of double-chained ammonium acetate surfactants. J. Phys. Chem. 95, 4777–4782.

Reed, W.F., 1994. A conformational interpretation for the peak of reduced viscosity for polyelectrolytes at low ionic strength. J. Chem. Phys. 100, 7825–7827.

Sacré, M.M., Tocanne, J.F., 1977. Importance of glycerol and fatty acid residues on the ionic properties of phosphatidylglycerols at the air-water interface. Chem. Phys. Lipids 18, 334–354.

Salonen, I.S., Eklund, K.K., Virtanen, J.A., Kinnunen, P.K.J., 1989. Comparison of the effects of NaCl on the thermotropic behaviour of *sn*-1′ and *sn*-3′ stereoisomers of 1,2-dimyristoyl-*sn*-glycero-3-phosphatidylglycerol. Biochim. Biophys. Acta 982, 205–215.

Tanford, C., 1961. The Physical Chemistry of Macromolecules. Wiley, New York.

Tocanne, J.F., Ververgaert, P.H.J.T., Verkleij, A.J., van Deenen, L.L.M., 1974. A monolayer and freeze-etching study of charged phospholipids. I. Effects of ions and pH on the ionic properties of phosphatidylglycerol and lysophosphatidylglycerol. Chem. Phys. Lipids 12, 201–219.

Tocanne, J.F., Tessié, J., 1990. Ionization of phospholipids and phospholipid-supported interfacial lateral diffusion of protons in membrane model systems. Biochim. Biophys. Acta 1031, 111–142.

Toko, K., Yamafuji, K., 1980. Influence of monovalent and divalent cations on the surface area of phosphatidylglycerol monolayers. Chem. Phys. Lipids 26, 79–99.

Träuble, H., Eibl, H., 1974. Electrostatic effects on lipid phase transitions: Membrane structure and ionic environment. Proc. Natl. Acad. Sci. USA 71, 214–219.

Träuble, H., Teubner, M., Wooley, P., Eibl, H., 1976. Electrostatic interactions at charged lipid membranes. I. Effects of pH and univalent cations on membrane structure. Biophys. Chem. 4, 319–342.

Wang, L., Bloomfield, V.A., 1991. Small-angle scattering of semidilute rodlike DNA solutions: polyelectrolyte behavior. Macromolecules 24, 5791–5795.

Watts, A., Harlos, K., Maschke, W., Marsh, D., 1978. Control of the structure and fluidity of phosphatidylglycerol bilayers by pH titration. Biochim. Biophys. Acta 510, 63–74.

Watts, A., Harlos, K., Marsh, D., 1981. Charge-induced tilt in ordered-phase phosphatidylglycerol bilayers. Evidence from X-ray diffraction. Biochim. Biophys. Acta 645, 91–96.

Yi, P.N., MacDonald, R.C., 1973. Temperature dependence of optical properties of aqueous dispersions of phosphatidylcholine. Chem. Phys. Lipids 11, 114–134.

Yin, J.J., Feix, J.B., Hyde, J.S., 1988. Solution of the nitroxide spin-label spectral overlap problem using pulse electron spin resonance. Biophys. J. 53, 525–531.

Zhang, Y.P., Lewis, R.N.A.H., McElhaney, R.N., 1997. Calorimetric and spectroscopic studies of the thermotropic phase behaviour of the *n*-saturated 1,2-diacylphosphatidylglycerols. Biophys. J. 72, 779–793.

Zimm, B.H., 1948. The scattering of light and the radial distribution function of high polymer solutions. J. Chem. Phys. 16, 1093–1116.